JOURNAL OF MATERIALS SCIENCE 29 (1994) 1765–1772

# Effect of size and morphology of particulate SiC dispersions on fracture behaviour of $Si_3N_4$ without sintering aids

G. PEZZOTTI
*The Institute of Scientific and Industrial Research, ISIR, Osaka University, 8-1, Mihogaoka, Ibaraki, Osaka 567, Japan*

T. NISHIDA
*Kyoto Institute of Technology, Faculty of Polytechnique Science, Department of Materials Engineering, Matsugasaki, Sakyo-ku, Kyoto 606, Japan*

The relation between microstructural characteristics and fracture behaviour of $Si_3N_4$/SiC-particle composites were evaluated for a series of materials containing a 25 vol% dispersion, with mean size in the range 7–106 μm. All the composites were fabricated by hot isostatic pressing without external addition of sintering aids via glass encapsulation. Quantitative image-analysis techniques were employed to assess the microstructural parameters, dealing with morphology and distribution of the SiC particles. A fracture mechanics analysis based on the determination of fracture strength, toughness, work of fracture and rising *R*-curve behaviour provided the basis for discussion of the effectiveness of the SiC dispersions. The results of mechanical tests are compared with those obtained on the monolithic material fabricated by the same process. The microfracture mechanisms in composites are discussed by relating microstructural data, obtained by image analysis, to toughness data.

## 1. Introduction

$Si_3N_4$ has received increasing attention as a possible replacement for the metallic superalloys in components for high-performance gas turbines, being capable, in principle, of operating without cooling at temperatures around 1400 °C. Among presently available $Si_3N_4$, materials sintered with small amount or without some sintering aids seem best to fit the requirements for deformation behaviour and subcritical-crack-growth resistance during long-term cycles at high temperature [1–4]. However, their marked brittleness still excludes these materials from consideration under conventional design practices [5–7].

This report describes an attempt to improve the fracture toughness of a highly refractory $Si_3N_4$ system by a brittle particulate dispersion. SiC particles of various sizes are systematically introduced in the $Si_3N_4$ matrix, and the composites sintered without external addition of sintering aids. Dense composite bodies are obtained by hot isostatic pressing. In addition to conventional measurements such as fracture strength, toughness and work of fracture, the microstructural parameters and *R*-curve behaviours were also determined. In an effort to improve understanding of the microfracture mechanisms in the present composite system, the quantitative microstructural data obtained by image analysis techniques were related to toughness data and rising *R*-curve behaviours of the composites. The interaction between the advancing crack and the composite microstructure was also examined, as it depends on the size and morphology of the SiC dispersion.

## 2. Experimental procedure

### 2.1. Materials fabrication

The matrix phase used in this study was a high purity, commercially available α-$Si_3N_4$ (E-10, Ube Industry, Tokyo, Japan). The reinforcing phase was α-SiC particles (GC 1500, 600, 320, 120, Showa Denko, Nagano Prefecture, Japan) whose mean size ranged between 7.2 and 106.0 μm. In Fig. 1, the particle-size distributions of the four SiC powders selected as reinforcement are shown, together with their mean size (i.e. size at 50% frequency). The SiC particle size was measured by a laser-transparency analyser after suspending the raw particles in ethylene glycol. Narrow particle distributions were obtained by an appropriate filtering process after mechanically grinding large SiC crystals. Four green bodies containing 25 vol % SiC particles were produced by wet-mixing the matrix and reinforcement starting powders in ethanol. A rotary evaporator containing Teflon-coated steel balls and immersed in an ultrasonic bath was employed to promote a thorough dispersion of powders. The performing cycle was performed by cold isostatic pressing (CIP) the powder mixtures at 200 MPa. The green densities obtained in this way were in the range

0022–2461  

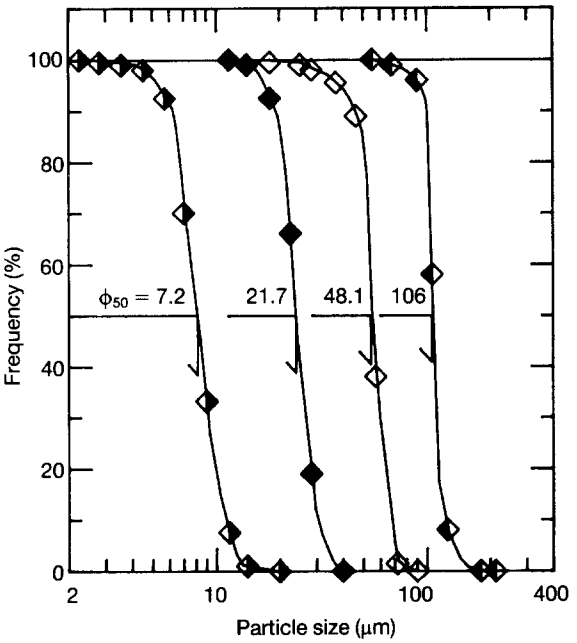


*Figure 1* Particle-size distributions of SiC raw powders as determined by laser-transparency analysis. Left-to-right, reinforcement of composites A to D.

45–50% for all the composites investigated. The pre formed bodies were coated with BN powder by a further CIP cycle and then prefired in vacuum ($10^{-5}$ Pa) at 1200 °C for 2 h to eliminate residual humidity. Specimens were encapsulated into borosilicate glass tubes evacuated to 0.1 Pa and hot-isostatically pressed (HIP) at 2050 °C for 2 h under 180 MPa pressure applied via Ar gas. The four sintered composite bodies containing particles of mean size 7.2, 21.7, 48.1 and 106.0 μm will hereafter be designated composites A, B, C and D, respectively. In the present study, the mechanical data for composites are compared with those of dense monolithic $Si_3N_4$ prepared by the same technique and HIP-sintered at 1950 °C for 2 h under 180 MPa [4, 6]. Bulk density values were determined using the Archimedes' displacement method and found to be > 99.5% of their theoretical values both in monolithic and composite specimens. Only β-$Si_3N_4$ and α-SiC phases were detected in the composite bodies by X-ray diffraction with Cu-$K_\alpha$ radiation. The monolithic sample constituted 100% β-$Si_3N_4$ phase. Microstructural data concerning the particle morphology and dispersion within the matrix were obtained on polished surfaces by automatically scanning with an image analyser. The total area investigated was about 4.0 $mm^2$ per composite.

## 2.2. Mechanical testing

Bend-bar specimens, 2 × 3 × 50 mm, were cut from the HIPed billets of each material and polished with 6-μm diamond paste, and the edges carefully removed. Measurements of fracture strength, $\sigma_f$, were carried out in four-point bending 10- and 40-mm spans. The cross-head speed was 0.5 mm $min^{-1}$. Eight specimens per material were tested.

Fracture toughness measurements were obtained using two methods: the single-edge V-notched beam (SEVNB) and the chevron-notch beam (CNB) methods. In the SEVNB method [8], a straight V-shaped sharp notch with a tip radius of about 16 μm was introduced along the longer section of the bending bars. The ratio between the flaw depth and the specimen thickness was 0.5. Tests were performed in three-point bending with a span of 45 mm. The $K_{Ic}$ values were calculated from the maximum load and the precracking length, and averaged on four specimens per material. Tests by the CNB method were conducted with the same loading arrangement as for the SEVNB tests. The cross-head speed was 0.002 mm $min^{-1}$. A deep chevron notch was cut with a thin diamond blade (slot 150 μm). The details of the notch geometry are shown in Fig. 2. The fracture initiation was revealed using an acoustic emission detector attached to the bending jig, and the crack length was calculated by compliance analysis using the Blumm's slice model [9, 10]. The $K_{Ic}$ value was calculated at the top of the load–displacement curve, from which the $K_R$ values for the successive crack extension (rising *R*-curve behaviour) were also obtained. The validity of the present method for measuring the rising *R*-curve behaviour of materials containing large extent particles has been discussed elsewhere [11]. A total crack length of about 750 μm was monitored. The obtained values were averaged among three specimens tested

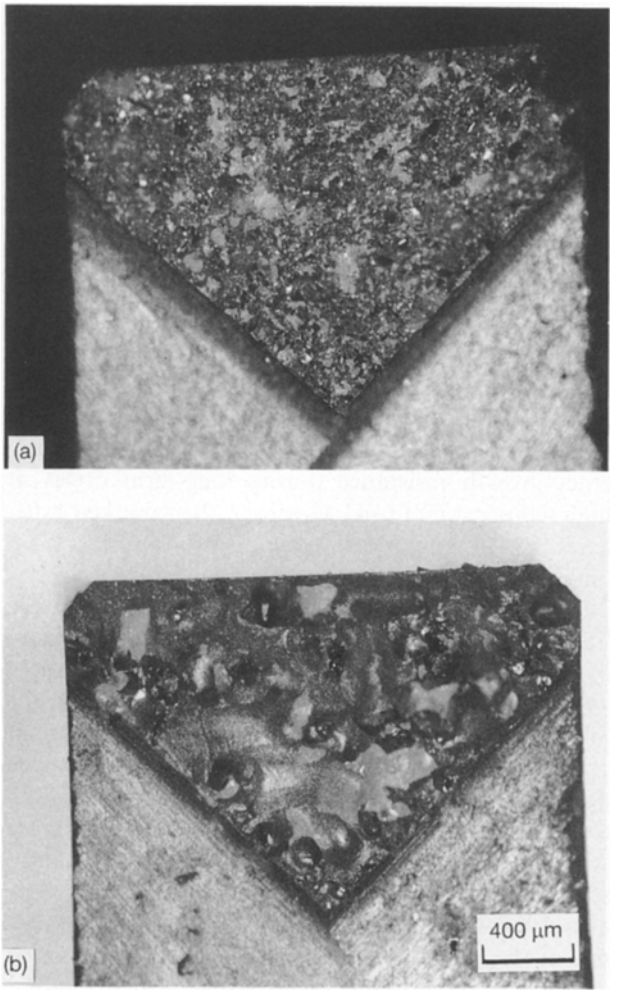


*Figure 2* Typical fracture surfaces of chevron-notched bars of composites C (top) and D (bottom) showing details of notch geometry and respective surface roughnesses.

for each material. The work of fracture was calculated by integrating the load–deflection curve and dividing by twice the fractured area. For comparison, $K_{Ic}$ values were also calculated from the work of fracture data using Irwin's similarity equation [12] (i.e. under the assumption of perfectly linear elastic material). In the calculation, the Young's modulus was 340 $\pm$ 5 GPa, as measured by the resonance vibration method in bending geometry.

## 3. Results

### 3.1. Morphology and distribution of SiC particles

A quantitative specification of the mean shape of the SiC particles was attempted by counting the number of edges on random sections. Typical optical images of polished composite surfaces used for image analysis characterization are shown in Fig. 3. The frequency of the number of edges, as determined for the particles in composite B, is shown in Fig. 4, and was found to be much closer to that of randomly distributed cubes (also shown in Fig. 4) than to standard data for other regular polyhedrons [13]. The average centre-to-centre near-neighbours distance (hereafter simply denominated interparticle distance, $\bar{\Delta}$) and its standard deviation were obtained in different composite specimens by lineal analysis [14, 15]. Data are plotted as a function of the mean particle size in Fig. 5. The average interparticle distance of regular polyhedrons can be expressed as a function of their edge length, $a$, as follows [16]:

$$\bar{\Delta} = \chi a / V_f \quad (1)$$

where $V_f$ represents the volume fraction of particles and $\chi$ is a known numerical shape coefficient [16]. The linear dependences on the edge length, as calculated for various regular polyhedrons, are also shown in Fig. 5. At particle sizes below approximately 50 μm, the experimental data seem to fit well with the theoretical line for the cubic shape, supporting the data obtained by edge counting (Fig. 4). On the other hand, the particles contained in composite D have a complex shape most probably affected by a higher irregularity. This fact may be a consequence of the grinding process. However, it should be noted that the standard deviation of the interparticle distance also becomes larger, reflecting the technological difficulties in finely dispersing large particles. Based on the above image analysis data, the present SiC particles will hereafter

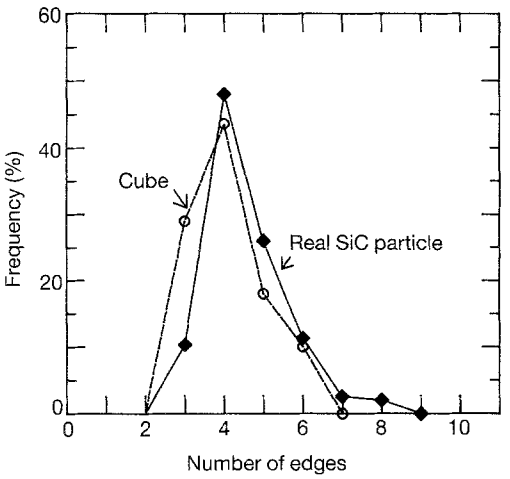


*Figure 4* Frequency of number of edges as determined for composite B in comparison with that of a regular cube.

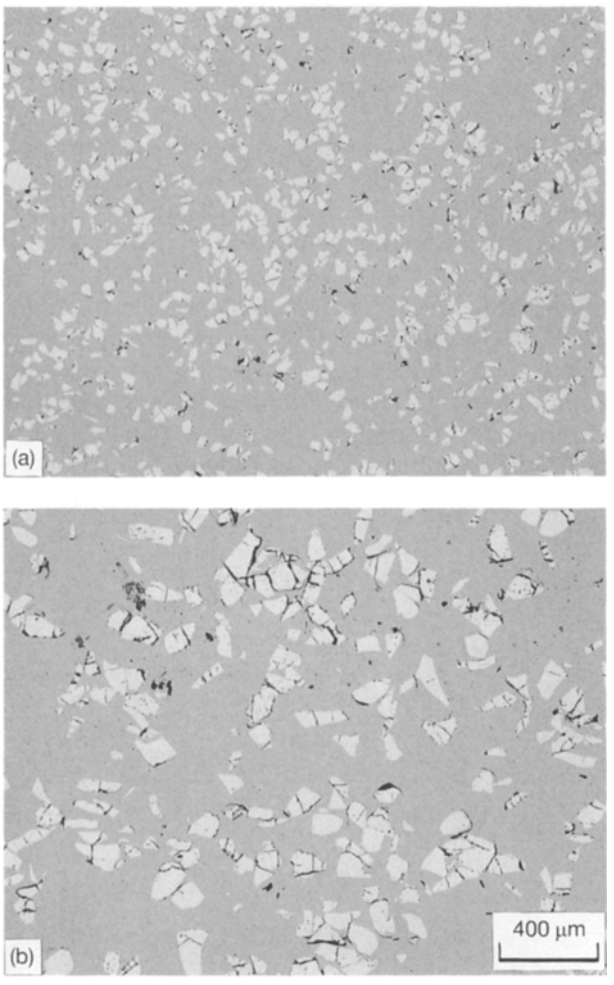


*Figure 3* Typical optical images of polished surfaces used for image analysis characterization of composites B (top) and D (bottom).

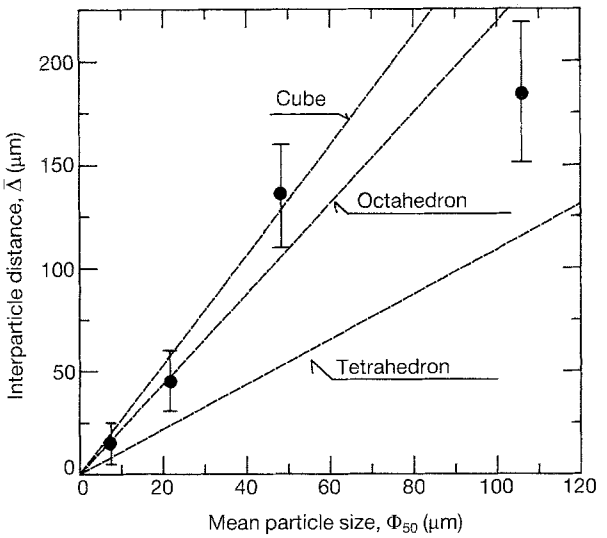


*Figure 5* Average interparticle distance as a function of mean particle size for various composites in comparison with theoretical linear dependences of regular monodispersed polyhedrons.

be considered as cube-shaped, with an edge length equal to their respective mean sizes.

### 3.2. Strength and toughness data

The mechanical properties of the composites are listed in Table I in comparison with the monolithic data. The dependence of fracture strength of the mean size of the added particles is also shown in Fig. 6, together with its scattering. As shown, the fracture strength dropped almost linearly with increasing particle size. Fractographic observations of composites C and D showed that large particles located near the tensile surface of the bend bars acted as the fracture origin (Fig. 7). It is therefore suggested that the low strength values measured in these composites reflect an inherent property of the materials, rather than being due to poor dispersion of the reinforcement.

A moderate increase in fracture toughness with increasing particle size was measured by different testing methods, while a similar but more marked trend (maximum increase in composite D > 150% of the matrix value) was found in the work of fracture data. This may suggest a better effectiveness of the SiC particles in enhancing toughening mechanism in the wake of the crack rather than those at the tip. This point will be discussed below. The contribution of the wake of the crack to toughening of the composites can be demonstrated by measuring their rising $R$-curve behaviours. As seen in Fig. 8, both composites A and B showed a flat behaviour, which suggests the inefficiency of small SiC particles in toughening the present highly refractory $Si_3N_4$. On the other hand, for additions of particles with mean size of 48.1 and 106.0 μm, the crack resistance was found to increase over a crack length of about 500 μm, and saturate at values about 15 and 45%, respectively, over the $K_{Ic}$ of the composites. In addition, fractographic observations of the CN specimens (Fig. 2), showing an increased surface roughness in these composites, confirm the occurrence of an improved microfracture mode. Contributions of crack bridging and friction during pulling out of particles may be responsible for such increases, as discussed below.

## 4. Discussion

### 4.1. Effectiveness of the SiC-particle dispersion

Due to the severe structural requirements to be satisfied during long-term operations at high temperatures, the amount as well as the composition of the grain boundary phase of $Si_3N_4$ cannot be arbitrarily changed. It is well known that the addition of sintering aids to $Si_3N_4$ can promote the growth of large acicular grains, and weaker the interfacial bonding, both these circumstances leading to markedly higher toughness values [17, 18]. However, the added sintering aid generally remains segregated at the grain boundary after sintering, and enhances degradation phenomena such as sliding and cavitation at elevated temperatures [19, 20]. The grain boundary of the present HIPed $Si_3N_4$ system, which is constituted by pure $SiO_2$ glass a few nanometres thick, has recently been the object of intensive studies [21–23] which demonstrate its highly refractory nature up to 1440 °C ($SiO_2$ is present as an impurity for about 2.4 wt % of the material. It is originated by surface oxidation of the starting $Si_3N_4$ powder after exposure to the atmosphere [4, 21]). On the other hand, as a consequence of the strong nature of the $SiO_2$ interface, no debonding (i.e. a fracture mode almost completely transgranular) is obtained, leading to very low toughness values. Detailed fracture analyses of the present monolithic $Si_3N_4$ have been described in previous reports [6, 7]. The present study confirms the difficulty of reinforcing the monolithic $Si_3N_4$ without sintering aids up to an acceptable level of toughness. SiC particles with sizes usually used in ceramic composites were ineffective, and only a moderate increase in fracture resistance could be achieved by adding large SiC particles. Such additions, however, considerably lowered the fracture strength of the material. It is clear that the dispersal of SiC in the present morphology and crystal structure is not worthwhile. Evidence in support of this assertion can be provided by observing the fracture mode on crack profiles introduced in the composites by Vickers indentation. Fig. 9 shows typical interactions between the advancing crack and the SiC particles, as observed in various composites. It is recognized that, independent of their morphology, SiC particles with size

TABLE I Mechanical properties of composites

| | $\sigma_f$ (MPa) | Work of fracture (J m$^{-2}$) | $K_{Ic}$ (MPa m$^{1/2}$) | | |
|---|---|---|---|---|---|
| | | | SEVNB | CN | Average work of fracture |
| Monolithic | 510 ± 35 | 10.7 ± 0.8 | 2.0 ± 0.3 | 2.4 ± 0.2 | 1.9 |
| Composite A ($\phi_{50}$ = 7.2 μm) | 615 ± 43 | 13.4 ± 1.0 | 2.4 ± 0.3 | 2.6 ± 0.2 | 2.2 |
| Composite B ($\phi_{50}$ = 21.7 μm) | 550 ± 57 | 16.0 ± 1.2 | 2.5 ± 0.4 | 2.8 ± 0.2 | 2.4 |
| Composite C ($\phi_{50}$ = 48.1 μm) | 414 ± 98 | 22.4 ± 2.0 | 2.9 ± 0.4 | 3.0 ± 0.4 | 2.8 |
| Composite D ($\phi_{50}$ = 106 μm) | 320 ± 64 | 27.8 ± 3.2 | 2.9 ± 0.4 | 3.2 ± 0.5 | 3.2 |

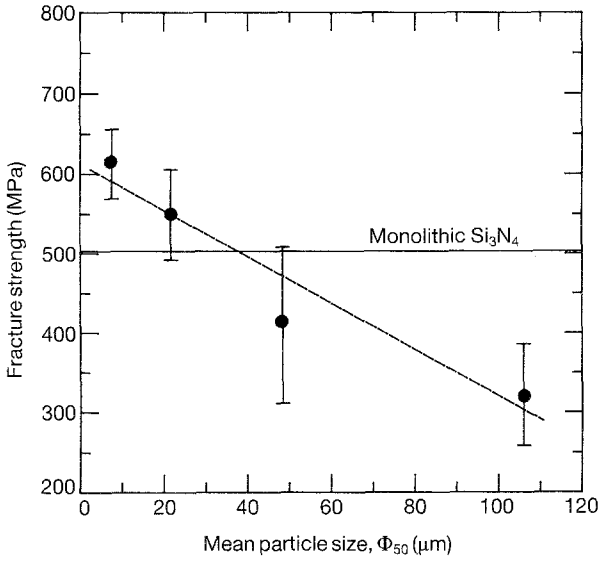


*Figure 6* Dependence of fracture strength of $Si_3N_4$ on mean size of added SiC particles.

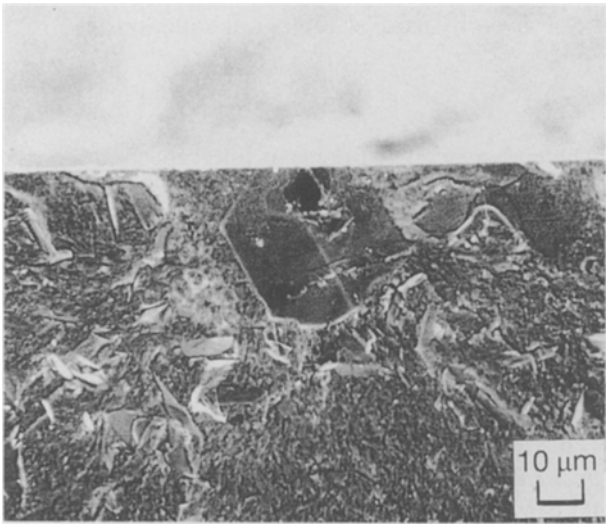


*Figure 7* Scanning electron micrograph of a typical fracture origin in composite D.

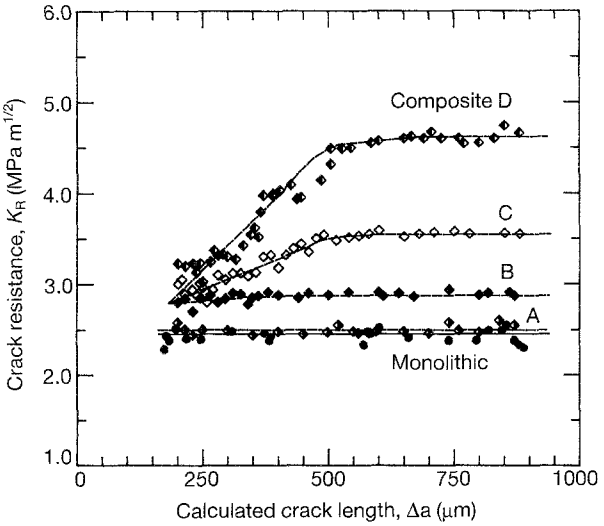


*Figure 8* Rising *R*-curve behaviour of composites A–D in comparison with that of the present monolithic $Si_3N_4$.

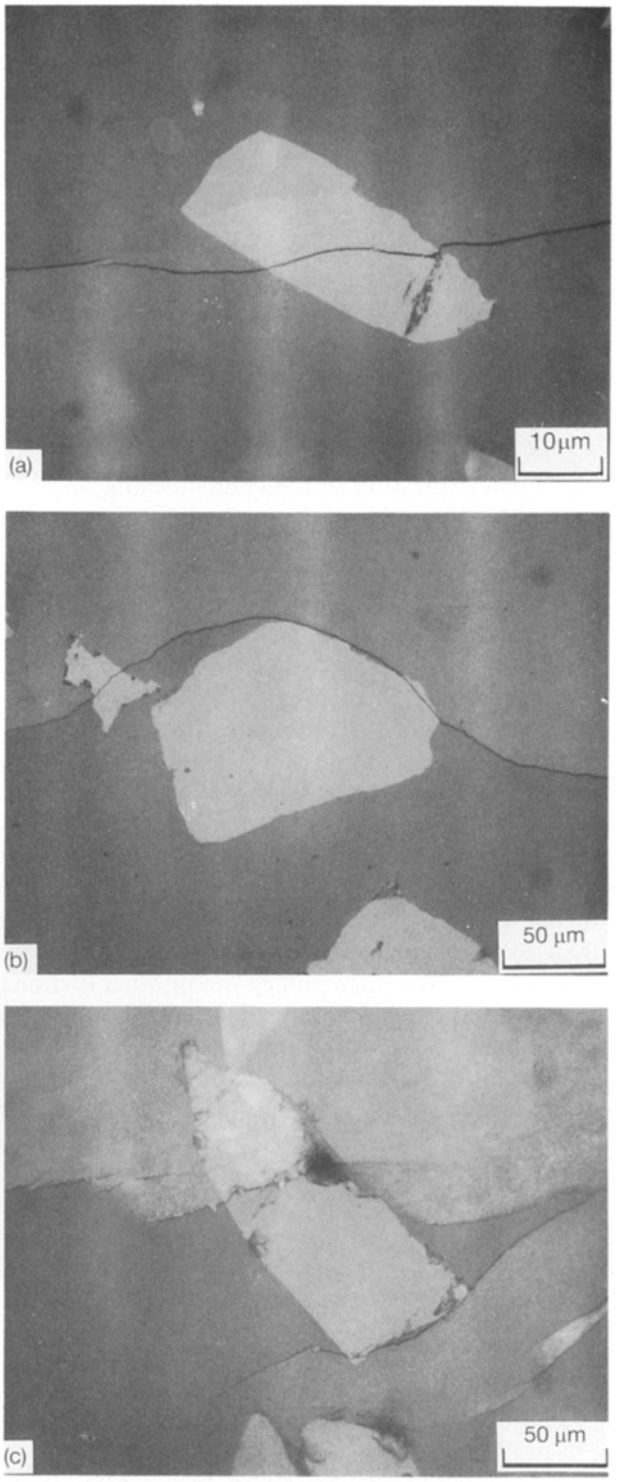


*Figure 9* Typical interaction between propagating crack and SiC particles, as observed by optical microscopy on crack profiles originated at the corners of a Vickers indentation.

< 20–30 μm fractured transgranularly without causing any apparent disturbance to the main crack path (Fig. 9a). On the other hand, large particles with rounded morphology were easily overcome by the advancing crack (Fig. 9b). This behaviour is in agreement with other fracture studies on brittle composites whose particulate reinforcement have a coefficient of thermal expansion larger than that of the matrix [24, 25], as in the present case. This kind of interaction is believed to make only a small contribution to toughening due to a slight misalignment of the crack

path. Slightly elongated particles (aspect ratio ~ 2–3) with a flat contour (plate-like shape) seem to be more effective in obstructing the advancing crack. The main crack path often showed branching and the particles were most probably fractured in the wake after being circumvented (Fig. 9c). This particles may contribute to the rising $R$-curve behaviour of the composites C and D.

## 4.2. Fractions of operative particles, tip and wake mechanisms

Under the hypothesis of uniform bridging traction, $\sigma_{br}$, in the wake of the advancing crack, the fracture mechanics expression of the crack-opening displacement, $\varphi^*$, at the edge of the stationary bridging zone can be given as [26]:

$$\varphi^* = 8(\Delta a^*/\pi)^{1/2}[\sigma_{br}(\Delta a^*/\pi)^{1/2} + (K_{Ic}/2^{1/2})] \quad (2)$$

where $E$ is the Young's modulus of the composite, and the parameter $\Delta a^*$ represents the stationary grain-bridging zone length as estimated from the rising $R$-curve dependence on the crack length (Fig. 8). This expression makes it possible to estimate the critical length of the grain bridges, $l^* = \varphi^*$. The resulting calculations for the present composites C and D show a value $l^* \sim 0.5$–$0.7$ μm. This value is relatively closer to the elongation-to-fracture of a single SiC particle than to its mean size, suggesting that the bridging mechanism, rather than pulling-out or other frictional phenomena, is the main operative mechanism in the crack wake. This result may be common for composites with a strong interfacial bonding. Furthermore, the values of $\Delta a^*$ as deduced from Fig. 8, in comparison with the respective interparticle distances, suggest that only a first array of particles behind the crack tip is able to operate bridging in the present composites. Based on this understanding, we can estimate the bridging traction, $\sigma_{br}$, and the effective fraction of particles operating bridging, $f_{br}$, (i.e. circumvented by the advancing crack front), using the following set of three equations [27]:

$$\sigma_{br} = \Delta k/2F(\xi)[a_0/\pi]^{1/2} \quad (3)$$

$$F(\xi) = [(1+\xi)^{3/2}/\xi][1 - 1/(1+\xi)^2]^{1/2} - [1/(1+\xi)] \times \arccos[1/(1+\xi)] \quad (4)$$

$$f_{br} = \sigma_{br}/V_f\sigma_p \quad (5)$$

where $a_0$ is the chevron notch depth and $F(\xi)$ is a numerical function of the relative crack extension, $\xi = \Delta a/a_0$. The strength of a single SiC particle was assumed to be $\sigma_p \sim 1$ GPa, in accordance with data in the literature [28–30]. The results of these calculations are shown in Fig. 10 as a function of the mean size of the added SiC particles. As shown, only a limited fraction of particles could be circumvented by the crack front and operated bridging in the crack wake (maximum fraction of about 40% in composite D). Obviously, the remaining fraction $f = 1 - f_{br}$ represents the particles fractured or surrounded at the crack tip (Fig. 9a and b). In the case of composite D, it may be also interesting to calculate the effective mean spacing, $\bar{\Delta}_{eff}$, between circumvented (unfractured) particles given by basic stereological equations as:

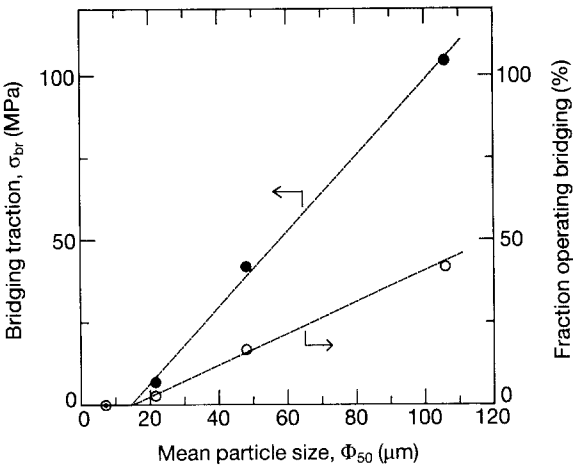


*Figure 10* Calculated dependences of bridging traction and fraction of particles operating bridging in the crack wake, as a function of the mean size of added SiC particles.

$$\bar{\Delta}_{eff} = 1/[(V_f f_{br}\bar{\Delta}/\bar{A}) - 1] \quad (6)$$

where $\bar{A} = 2a^2/3$ is the mean intercept area for randomly oriented cubes [16]. Substituting in Equation 6 the parameters appropriate for composite D and the value of $f_{br}$ found by using Equations 3–5, we can estimate $\bar{\Delta}_{eff} \sim 0.8$ mm. This large value of $\bar{\Delta}_{eff}$, compared with the mean particle size, would suggest a negligible contribution by crack front bowing (or pinning) as a toughening mechanism operating at the crack tip.

A simplified account of the toughening achieved under the effect of mechanisms operating at the crack tip can be given as follows. The toughening achieved by bowing between particles and eventually circumventing them is given by the rule of mixtures in the first approximation as [31]:

$$K_{Ic} = \{\bar{\Delta}(K_{Ic}^m)^2 + L[(K_{L_{max}})^2 f_{br} + (\bar{K}_L)^2(1 - f_{br})]/(\bar{\Delta} + L)\}^{1/2} \quad (7)$$

where $K_{Ic}$ and $K_{Ic}^2$ are the fracture toughness of the composite and that of the matrix, respectively, and $L = 2a/3$ is the mean intercept length for an array of randomly distributed cubes [16]. Assuming a negligible difference between the moduli of matrix and particles, numerical solutions for the crack-tip toughness contribution by completely circumvented particles, and particles operating a partial bowing of the advancing crack front before being fractured, have been given for the present $V_f$ value by Fares [32] as $K_{L_{max}}/K_{Ic}^m = 2.35$ and $\bar{K}_L/K_{Ic}^m \sim 1.25$, respectively. Introducing these values in Equation 7, we can, for example, calculate for the composite D $K_{Ic} = 2.6$ MPam$^{1/2}$, which is in good agreement with the experimental data and provides the rationale for the low increase in toughness with respect to the matrix.

### 4.3. Maximum predicted toughening for strongly bonded particles

Finally, it is interesting to estimate for the present system the maximum toughening achievable by particulate reinforcement, when the fraction of particles totally circumvented at the tip and operating bridging in the wake approach unity ($f_{br} = 1$). Still considering the presence of a strong interfacial bonding, which makes the frictional contribution negligible by pulling out particles, and allows the hypothesis of only a single array bridging the crack, a maximum value of composite $K_{Ic} = 3.6$ MPam$^{1/2}$ can be calculated from Equation 7. On the other hand, a saturated value of $K_R = 9.6$ MPam$^{1/2}$ (corresponding to a maximum bridging traction, $\sigma_{br} \sim 250$ MPa) after a complete development of the bridging zone, is found from Equations 3 and 4. The results of these orientative calculations suggest that SiC particles in the present morphology can make a marked contribution as bridging ligaments, while they may have only a minor effect in obstructing the advancing crack front. The present study also suggests that a shape containing flat surfaces may be more effective in toughening, as it is not easily overcome by the crack tip and, once circumvented by it, leads to bridging. Furthermore, it should be noted that, for example, a disc-shaped particle will have a mean intercept length twice that of a spherical particle with the same volume and radius, and three times larger than a cubic particle with the same volume and edge equal to its radius [16]. This means that, for the same added $V_f$ of second phase, the portion of crack front subjected to obstruction is significantly larger in the case of discs; i.e the interparticle distance is drastically reduced. Both the above observations imply that a better crack-tip toughening effect can be obtained in the present composite by adding platelets of appropriate size (to avoid cleavage fracture at the tip) rather than particles. Further experimental results regarding the fracture behaviour of the present $Si_3N_4$ reinforced by SiC platelets, and confirming the present conclusions, are described elsewhere [33, 34].

## 5. Conclusions

The attainment of an actual reinforcement by SiC dispersion in brittle $Si_3N_4$ matrix was found to depend markedly upon both the size and morphology of the dispersion. According to quantitative image analysis and fracture mechanics experiments, it was found that, for a polyhedric shape of the SiC particles (as in the present case), a large size (50–100 μm) is required to avoid transgranular fracture at the crack tip and to obtain some toughening effect. However, the toughness increase was relatively small (after full development of the bridging zone $K_R \sim 2K_{Ic}^m$ and work of fracture 2.5 times that of the matrix) and was accompanied by a drastic reduction ( $\sim 40\%$) in the inherent strength of the material. These results may be somewhat general for $Si_3N_4$-based composites with a strong interfacial bonding. In accordance with basic stereological equations and fractographic observations, the present SiC main morphology was found not to be suitable for obstructing the advancing crack front. Some particles containing flat surfaces, whose shape was closer to platelets, appeared to be more effective for such purpose. In the present composite system, the maximum achievable $K_{Ic}$ for zero fraction of transgranularly fractured SiC particles was calculated as $\sim 3.6$ MPa m$^{1/2}$ by extrapolating the available fracture data. On the other hand, a higher increase ($K_R \sim 9.6$ MPa m$^{1/2}$) of crack resistance by the saturated bridging zone could be predicted, suggesting the greater effectiveness of SiC particles in toughening by crack-wake mechanisms.

## Acknowledgements

The authors wish to express their thanks to Professor K. Niihara for providing the research facilities at ISIR, Osaka University. One of the Authors (G.P.) was financially supported by the Japan Society for the Promotion of Science (JSPS).

## References

1. H. LARKER, J. ADLERBORN and H. BOHMAN, Society of Automotive Engineers, Technical paper No. 770335 (1977).
2. J. HEINRICH and M. BOEHMER, *Ber. Dtsch. Keram. Ges.* **61** (1984) 399.
3. K. HONMA, H. OKADA, T. FUJIKAWA and T. TATSUNO, *Yogyo-Kyokai-Shi* **95** (1987) 229.
4. I. TANAKA, G. PEZZOTTI, T. OKAMOTO, Y. MIYAMOTO and M. KOIZUMI, *J. Amer. Ceram. Soc.* **72** (1989) 1656.
5. J. ADLERBORN, M. BURSTROEM, L. HERMANSSON and H. LARKER, *Mater. Design* **8** (1987) 229.
6. I. TANAKA, G. PEZZOTTI, Y. MIYAMOTO and T. OKAMOTO, *J. Mater. Sci.* **26** (1991) 208.
7. G. PEZZOTTI, I. TANAKA and T. NISHIDA, *Phil. Mag. Lett.* **67** (1993) 95.
8. H. AWAJI and Y. SAKAIDA, *J. Amer. Ceram. Soc.* **73** (1990) 3522.
9. J. I. BLUHM, *Eng. Fract. Mech.* 7 (1975) 593.
10. Appendix in D. MUNZ, T. T. BUBSEY and J. L. SHANNON, Jr., *J. Amer. Ceram. Soc.* **63** (1980) 300.
11. G. PEZZOTTI, K. NIIHARA and T. NISHIDA, *J. Test. Eval.* **21** (1993) 358.
12. G. R. IRWIN, *J. Appl. Mech.* **24** (1957) 361.
13. F. C. HULL and W. J. HOUK, *Trans. AIME* **197** (1953) 565.
14. E. E. UNDERWOOD, "Quantitative Stereology" (Addison-Wesley, Massachussetts, 1970) p. 26.
15. G. PEZZOTTI, I. TANAKA and T. OKAMOTO, *J. Amer. Ceram. Soc.* **73** (1990) 3033.
16. E. E. UNDERWOOD, "Quantitative Stereology" (Addison-Wesley, Massachusetts, 1970) p. 92.
17. E. TANI, S. UMEBAYASHI, K. KISHI, K. KOBAYASHI and M. NISHIJIMA, *Amer. Ceram. Soc. Bull.* **65** (1986) 1311.
18. C. W. LI and J. YAMANIS, *Ceram. Eng. Sci. Proc.* **10** (1989) 632.
19. J. A. TODD and Z. Y. XU, *J. Mater. Sci.* **24** (1989) 4443.
20. R. L. YECKLEY and K. N. SIEBEIN, in "Proceedings of the Third International Symposium on Ceramic Materials and Components for Engines", edited by V. J. Tennoy (American Ceramics Society Ohio, 1989) p. 751.
21. I. TANAKA, G. PEZZOTTI, K. MATSUSHITA, Y. MIYAMOTO and T. OKAMOTO, *J. Amer. Ceram. Soc.* **74** (1991) 752.
22. I. TANAKA and G. PEZZOTTI, *ibid.* **75** (1992) 772.
23. *Idem, ibid.* **75** (1992) 1023.
24. R. W. DAVIDGE and D. J. GREEN, *J. Mater. Sci.* **3** (1968) 629.
25. N. MIYATA and H. JINNO, *ibid.* **16** (1981) 2205.

26. G. C. SIH, "Handbook of Stress Intensity Factors" (Lehigh University Press, Pennsylavania, 1973).
27. M. SAKAI and R. C. BRADT, *Seramikkusu Rombunshi* **96** (1988) 801.
28. D. P. H. HASSELMAN and H. D. BATHA, *Appl. Phys. Lett.* **2** (1963) 111.
29. J. J. PETROVICH, J. P. MILEWSKI, D. L. ROHR and F. D. GAC, *J. Mater, Sci.* **20** (1985) 1167.
30. H. KATSUKI, H. USHIJIMA, M. KANDA, H. IWANAGA and M. EGASHIRA, *Yogyo-Kyokai-Shi* **95** (1987) 1089.
31. L. R. F. ROSE, *Mech. Mater.* **6** (1987) 11.
32. N. FARES, *J. Appl. Mech.* **56** (1989) 837.
33. G. PEZZOTTI, *J. Amer. Ceram. Soc.* **76** (1993) 1313.
34. G.PEZZOTTI, K. NODA, Y. OKAMOTO and T. NISHIDA, *J. Mater. Sci.* **28** (1993) 3080.

*Received 10 October 1992*
*and accepted 21 September 1993.*